Full Length Article

Interpass rolling of Ti-6Al-4V wire + arc additively manufactured features for microstructural refinement

Anthony R. McAndrew[a], Marta Alvarez Rosales[a], Paul A. Colegrove[a,*], Jan R. Hönnige[a], Alistair Ho[b], Romain Fayolle[a], Kamal Eyitayo[a], Ioan Stan[a], Punyawee Sukrongpang[a], Antoine Crochemore[a], Zsolt Pinter[a]

[a] Cranfield University, Cranfield, Bedfordshire, MK43 0AL, UK
[b] University of Manchester, Manchester, Greater Manchester, M13 9PL, UK

ABSTRACT

In-process deformation methods such as rolling can be used to refine the large columnar grains that form when wire + arc additively manufacturing (WAAM) titanium alloys. Due to the laterally restrained geometry, application to thick walls and intersecting features required the development of a new 'inverted profile' roller. A larger radii roller increased the extent of the recrystallised area, providing a more uniform grain size, and higher loads increased the amount of refinement. Electron backscatter diffraction showed that the majority of the strain is generated toward the edges of the rolled groove, up to 3 mm below the rolled surface. These results will help facilitate future optimisation of the rolling process and industrialisation of WAAM for large-scale titanium components.

1. Introduction

Wire + arc additive manufacturing (WAAM) is a 3D printing technology capable of meeting the needs of industry for producing metre-sized metallic components [1]. These components are produced through layer by layer material deposition, utilising an arc-based heat source, such as plasma or Metal Inert Gas deposition, and wire as feedstock [2,3]. Fig. 1 illustrates the process.

Owing to the many benefits of WAAM (e.g. high deposition rate, manufacturing cost reduction and reduced lead time) it is finding increasing interest for the manufacture of aircraft structural components – particularly for Ti-6Al-4V. This is primarily due to titanium and its alloys being extremely expensive in terms of purchase cost ($> £70 \, kg^{-1}$), energy consumption ($> 500 \, MJ \, kg^{-1}$) and CO_2 emissions ($> 40 \, kg \, kg^{-1}$) [4]. Typically, Ti-6Al-4V aircraft structural components are machined from oversized ingots, forgings and extrusions. Not only is this a time consuming process (e.g. waiting for forging dies to be manufactured) but it is also expensive due to the proportionally large amount of material that is purchased compared to the amount that remains after machining. The buy-to-fly (BTF) ratios of components manufactured using this approach can be as poor as 20:1. WAAM reduces the material required to make a component by producing near-net-shape preforms, which are subsequently machined to the desired

dimensions. This brings substantial improvements to the BTF ratios (typically 1.5), which significantly reduce the manufacturing cost [2].

For successful implementation of WAAM the material properties should ideally meet or exceed those from the wrought material. This can be difficult due to the very different manufacturing route that AM parts undergo – normally they experience a series of thermal cycles with ever decreasing peak temperatures. For Ti-6Al-4V WAAM the small freezing range and epitaxial growth results in large, columnar prior β grains that have anisotropic properties, which are undesirable for aerospace applications [2,5].

Colegrove et al. [6] described how interpass rolling of the deposited layers can improve the mechanical properties of Ti-6Al-4V WAAM deposits through microstructural refinement of the prior β grains. Interpass rolling increased both the yield and tensile strengths by 18–25% while eliminating material anisotropy. An equiaxed prior β microstructure that can be as small as 60 μm is produced despite the induced strain being relatively modest (7–20%) [9,10]. Interpass rolling also improves fatigue properties due to the high proof strength, fine Widmanstatten basket-weave microstructure and isotropic texture with a small prior β grain size [6,7]. The improvement may also be due to the reduced incidence of porosity [8] which is known to limit fatigue performance [9].

An early investigation showed that prior β refinement initiates on

---

* Corresponding author.
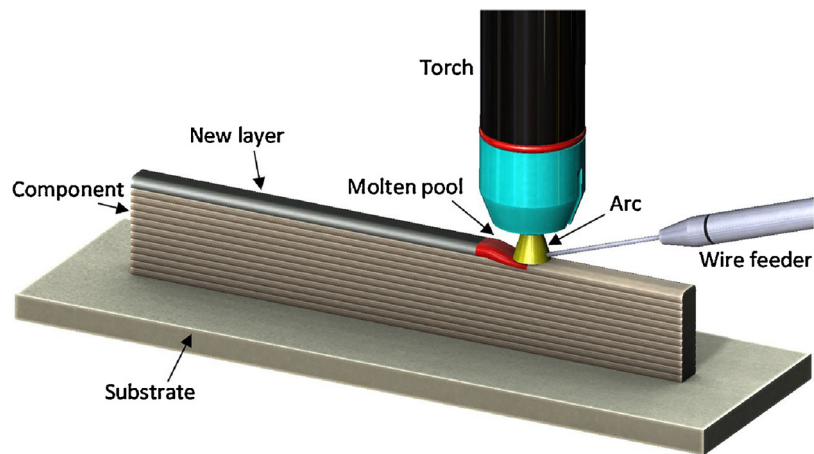 *E-mail address:* p.colegrove@cranfield.ac.uk (P.A. Colegrove).

Fig. 1. Illustration of the WAAM process.

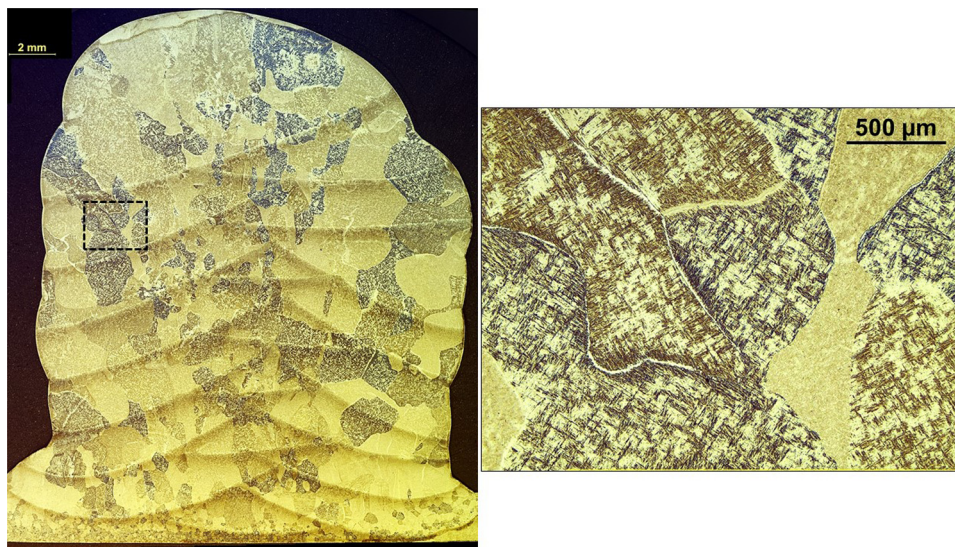**Fig. 2.** A macrograph of a thick Ti-6Al-4V WAAM wall that was rolled with a flat roller at 75 kN. Notice that there is little prior β grain refinement.
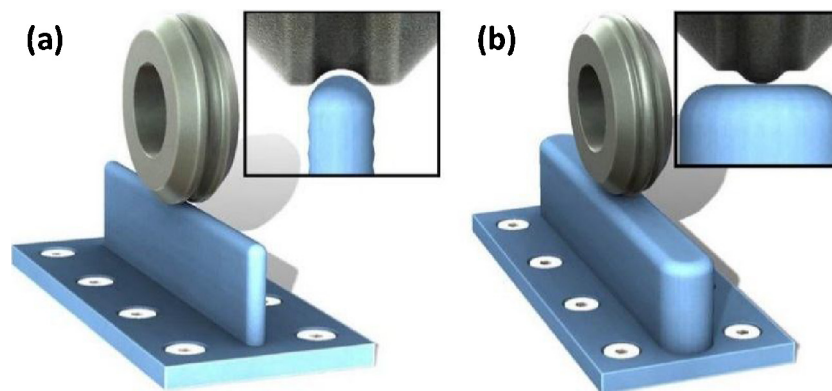

Fig. 3. Schematic diagram of the main rolling methods: (a) vertical with a profiled roller; (b) rolling with an inverted profiled roller for thick sections and intersections.

twinned α colonies upon heating [10], but more recent work reports that the new β orientation originate from twinned β cells; because the β phase grows from residual β between the α laths before new β can nucleate in pure (i.e. twinned) α at higher temperature [11]. The large number of β nuclei with random orientation prevent the re-establishment of the previous columnar microstructure.

A number of different rolling methods have been developed.

Interpass rolling has predominantly been applied to thin (< 10 mm) walls and the rollers often have a similar profile to the deposit [7,12] (Fig. 3(a)). Martina et al. [7] demonstrated that similar levels of refinement were possible with a flat roller, however the grains were smaller in the centre of the wall due to the concentration of strain in this region. Applications that involve thin walls have very little lateral restraint, so strain can be relatively easily induced within the material:
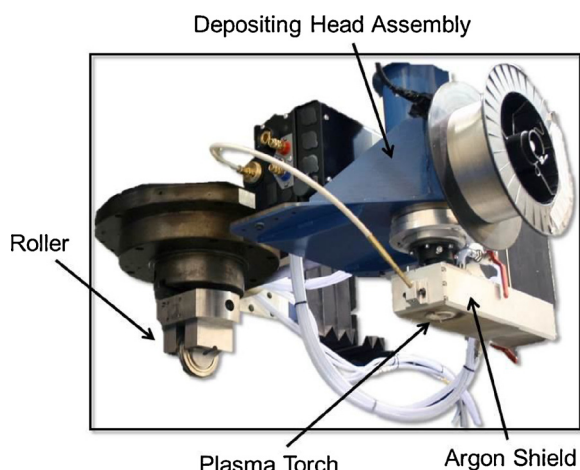
Fig. 4. HiVE machine showing deposition torch and spindle with roller assembly.

Table 2
Deposition parameters.

Deposition layer number	1–3	4–12
Wire feed speed (WFS)	2.2 m/min	2.4 m/min
Travel speed (TS)	200 mm/min	200 mm/min
Current	200 A	190 A
Argon gas flow	195 l/min	195 l/min
Torch stand-off distance	8 mm	8 mm

a large vertical plastic compressive strain produces an almost equal in magnitude and tensile lateral strain. Zhang et al. [13] and Zhou et al. [14] applied the technique 'in situ' to thin steel walls, and also achieved significant levels of grain refinement. Xie et al. [15] demonstrated the application of pinch rollers which were applied just prior to a flat roller. The equipment was termed 'a miniature metamorphic rolling mechanism' and it allowed accurate and flexible control of the final part geometry. Finally, Hönnige et al. [16] applied side rolling to Ti-6Al-4V walls: after the wall was built it was rotated onto its side and it was deformed with a large flat roller, which was extremely effective for removing residual stress and distortion.

A preliminary investigation into the rolling of a thick (approximately 18 mm wide) wall with a flat roller was conducted at Cranfield University. As shown in Fig. 2, application of a 75 kN load did not produce any significant grain refinement due to the greater level of lateral restraint with this geometry. i.e. it is difficult to induce the required strain for microstructural refinement. Consequently, in this paper we investigate whether an inverted profile roller – as shown in Fig. 3(b) – generates the large strains required for grain refinement. This will be applied to intersections and thick walls produced by WAAM and are contained in most applications.

2. Methodology

The work was done in three parts: the first involves the production of "thick" Ti-6Al-4V walls; the second involves the production of intersecting features; and finally electron beam back scattered diffraction (EBSD) was used to generate strain maps of the rolled material. The purpose of the EBSD work is to aid understanding of how the rollers impart strain into the samples.

2.1. Thick walls

The samples were manufactured on the HiVE (High-Value Engineering) centre at Cranfield University: a roller is placed in the spindle of a large CNC machine which allows multi-directional rolling with loads up to 100 kn. This machine is shown in Fig. 4 and is also equipped with plasma deposition equipment that allows the wire to rotate around the torch to facilitate deposition in multiple directions. A

Fronius Plasma 10 module and Fronius TIG 5000 Series power supply were used for the plasma deposition. A torch stand-off distance of 8 mm was used, and φ1.14 mm Ti-6Al-4V wire was fed at an angle of 45° into the arc. The composition of the wire is shown in Table 1. A local shielding device (WAAM-Shield) was used to prevent the hot titanium oxidising [17], and used an argon gas flowrate of 195 l/min.

To produce the "thick" walls, three parallel deposits were overlapped by 50% of the single pass wall width (11 mm). The middle deposit was deposited first and then another two passes were deposited on either side. As a result of the overlap, the three deposited passes made a total layer height of 1.65 mm and a wall width of 22 mm. The wall was deposited to a length of 150 mm and the parameters used to make the individual deposits are shown in Table 2. The walls were deposited on 12.7 mm thick Ti-6Al-4V substrates, and the deposition direction was alternated each layer to provide a uniform layer height across the wall; without this, a hump is produced where the arc is ignited and a depression is produced at the end which accumulates with each deposited layer. After each deposited pass, the local shielding device continued to provide protection for 45 s to provide protection while the deposit cooled below a temperature where oxidation readily occurs (400 °C).

One sample was produced without rolling. The remaining six used the three roller profiles shown in Fig. 5 with loads of 60 kn and 90 kn. Since flat and profiled rollers are unable to produce the required strain and grain refinement in thick walls (Fig. 2), the rollers in Fig. 5 used an inverted profile to produce a more concentrated load that will hopefully produce greater subsurface strain and refinement. The rollers were manufactured from H13 tool steel with a hardness of 42–44 HRc. Interpass rolling was applied along the same coordinate path as the deposition passes at a speed of 2000 mm/min, i.e three roller passes occurred per layer. It was applied once the deposit was near room temperature (< 100 °C) and the last deposited layer (i.e. layer 12) was not rolled.

For the metallographic analysis, 10 mm thick samples were cut across the length of the WAAM walls using a vertical cutting machine. The sections were obtained from the middle of the manufactured walls to guarantee the stability of the deposition process. The sections were hot mounted in a Ø40 mm phenolic resin then ground with 120, 240, 1200 and 2500 grit papers. Polishing was performed with a solution of oxalic acid and water based colloidal silica suspension. Finally, samples were etched using a diluted hydrofluoric acid solution. An optical microscope was used to obtain the microstructural images that were stitched together with Microsoft Image Composite Editor. The average grain size was determined with the Planimetric Method described in ASTM E-112.

2.2. Intersections

The intersection samples were also produced on the HiVE using a local shielding device. The wire type and feed position were kept the
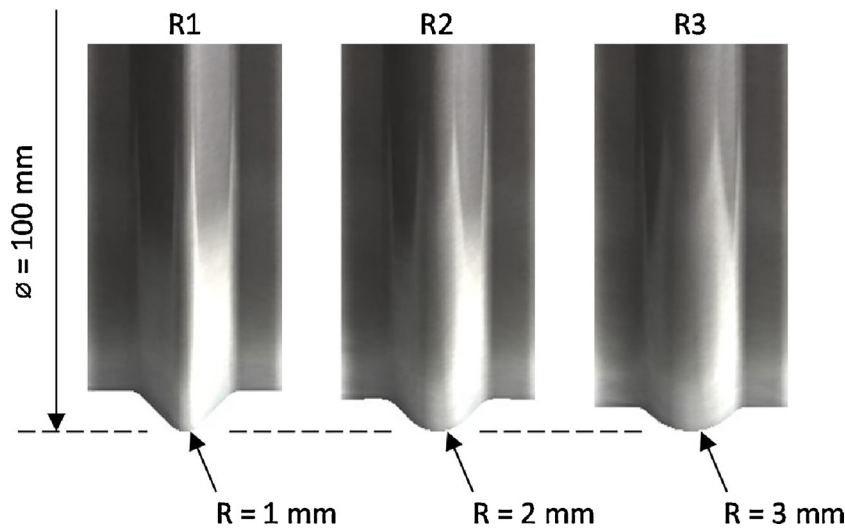
Table 1
Ti-6Al-4V wire composition.

Ti	Al	V	Fe	O	C	N	H	Y	Others
Remainder	5.50–6.75	3.5–4.50	0.22	0.12–0.18	0.05	0.030	0.015	0.005	0.2

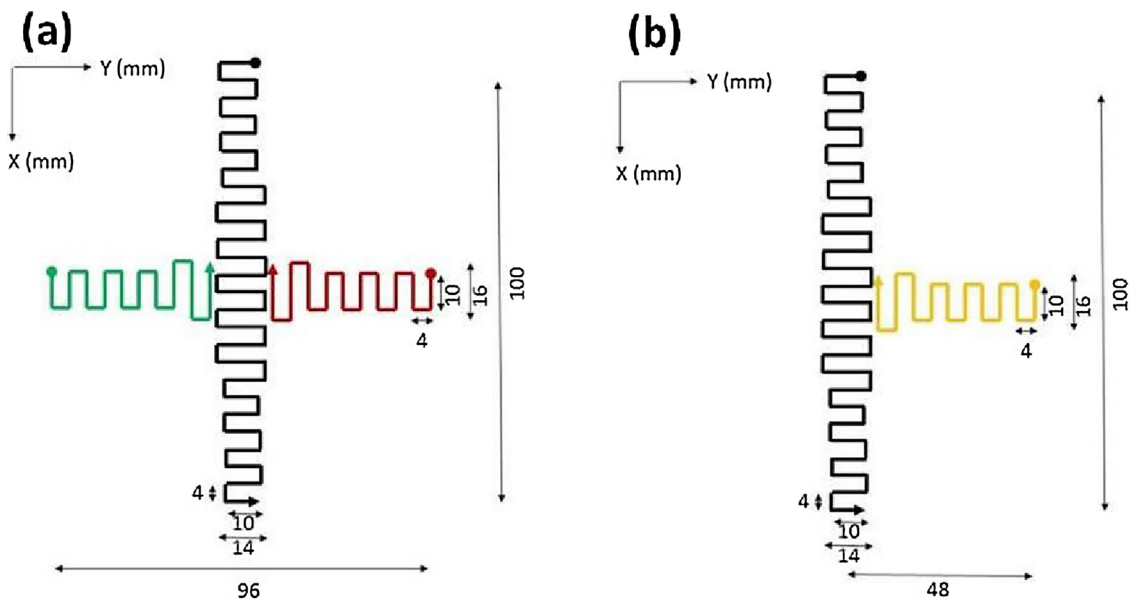**Fig. 5.** Roller types used for the experimental study.

Fig. 6. Deposition paths for the (a) cruciform and (b) tee intersections. Note direction of deposition is alternated every second layer.

Table 3
Intersection types.

Intersection type	Intersection label	Rolling strategy
Cruciform Intersection	CSX	Unrolled
	R1X	One rolling pass
	R2X	Two rolling passes
Tee Intersection	CST	Unrolled
	R1T	One rolling pass
	R2T	Two rolling passes

Fig. 7. Schematic of the extraction for the plastic strain measurement specimen and location of the profiled rolling pass.

same and two types of intersections were manufactured: a cruciform and a tee. The intersections were composed of 16 mm wide and 20 mm high walls deposited with an oscillation strategy on 180 mm × 180 mm × 12.7 mm substrates – see Fig. 6. The deposition paths involved depositing first the black wall and then, the red and green walls. At the intersecting area the wall width was increased to 22 mm to widen the material overlap enabling a radii to be machined for the final part. The dimensions of the path are shown in Fig. 6 and the path was reversed every second layer to obtain a flat intersection that assisted the subsequent rolling process. Due to the proprietary
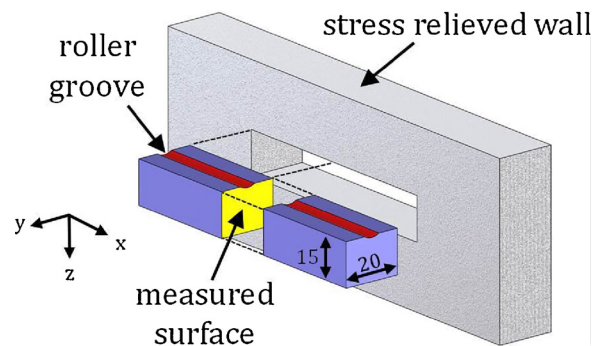
nature of these parameters, they cannot be disclosed; however they produced a layer height of approximately 1.5 mm and a bead width of approximately 6 mm. Local shielding was used as for the previous experiments.

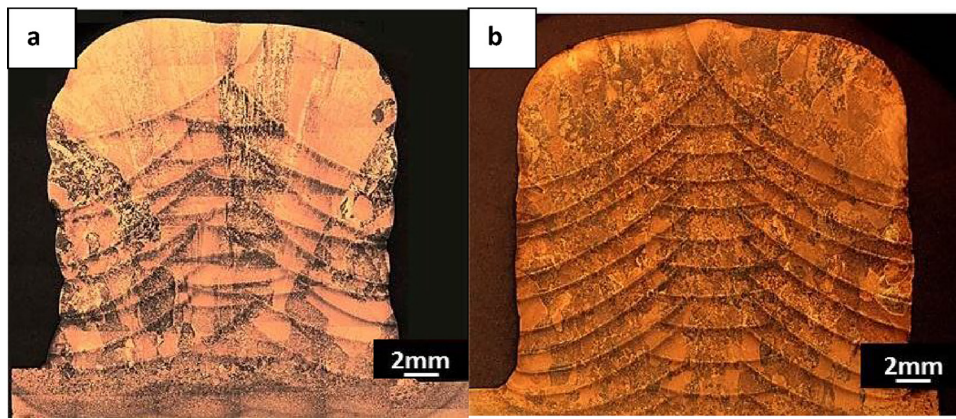Table 3 summarises the rolling strategies used for the cruciform and

Fig. 8. Comparison between (a) control and (b) sample rolled with a 60 kN load and a roller with a radii of 3 mm.
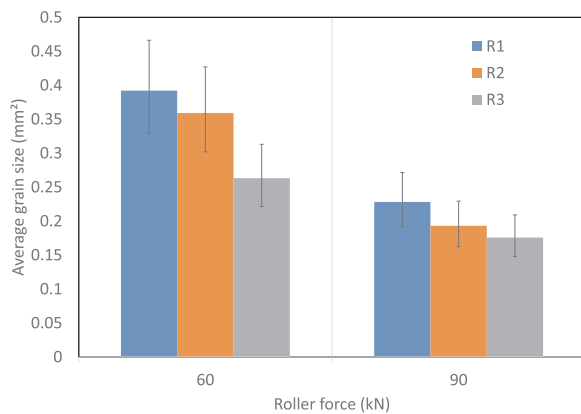

Fig. 9. Mean prior β grain size according to the Planimetric Method (ASTM E-112) for the different roller types and forces.

tee intersections. Two rolling strategies were carried out: with one and two rolling passes. In each case a rolling load of 75 kN at a speed of 2000 mm/min was applied with the 3 mm radius roller shown in Fig. 5. The single rolling pass was applied to the centreline of the deposit, while the two rolling passes were done parallel to each other and offset from the centreline by 3 mm, leaving a 6 mm gap between the two rolling passes. Every layer the rolling path directions were reversed and it was applied after the deposit was near room temperature (< 100 °C).

For the metallographic analysis, a sample was extracted from a planar cross-section of each intersection. Analysis of the sections was identical to the thick wall samples in 2.1.

2.3. EBSD and strain mapping

A 20 mm wide, 15 mm high and 80 mm long section of an unrolled

and stress relieved (4 h at 650 °C in an inert atmosphere) Ti-6Al-4V wall was extracted, as shown in the schematic in Fig. 7. One rolling pass along the centreline on the top surface of the specimen was produced using the R3 roller with 90 kn. The measured surface was located in the y-z plane in the centre of the specimen.

After mounting in conductive resin, the surface was treated with similar sample preparation to that already mentioned, including polishing, but without etching. Scanning electron microscopy (SEM) and electron back scatter diffraction (EBSD) were used to produce the inverse pole figure (IPF) map of the α-phase, using the Maxim FEG-SEM by CamScam and the Aztec acquisition software to process the data from the Oxford instruments EBSD system. To incorporate the 4 mm wide roller groove and the estimated depth of the penetration, an area 6.37 mm wide and 4.82 mm high was scanned with an EBSD step size of 6 μm in the top centre of the 20 mm by 15 mm cross-section. The Ti-6Al-V alloy typically contains a low volume fraction of only 5–9% of the high temperature bcc β-phase [18]. Davies et al. [19,20] have developed a procedure that can reconstruct the IPF of the parent β-phase at elevated temperatures, using the Burger orientation relationship (BOR). According to BOR the hexagonal close packed (hcp) α-phase transforms with the basal {0001} plane upon cooling on the most densely packed {110} plane of the parent body-centred-cubic (bcc) β-phase. The detailed β-reconstruction procedure is explained elsewhere [21].

To identify the region that each of the rolling passes deforms plastically, a plastic strain map was produced using the compiled EBSD data. They were produced using information from the regions where the previously explained β-reconstruction was not successful: after performing the β-reconstruction procedure six times with gradually changing tolerated deviation angle between 1° and 6° of neighbouring α-laths [22], certain areas could not be reconstructed. A high tolerance angle during the application of the technique allows the reconstruction of more parent β–phase orientations, while a small tolerance can only reconstruct regions with only little deviation of neighbouring α-laths. Since plastic strain is responsible for deviation within the α-colonies,
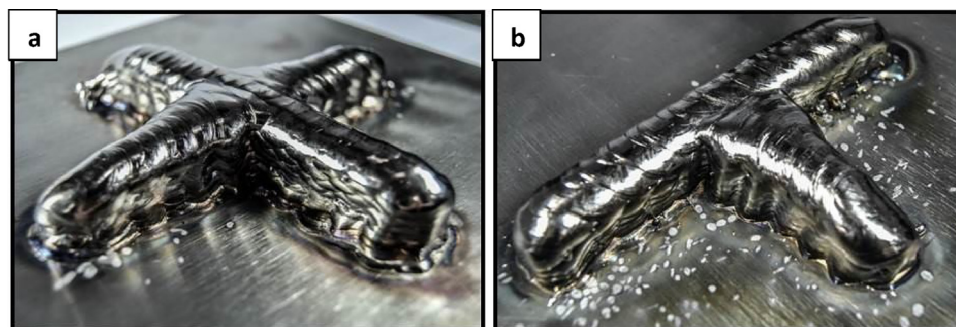

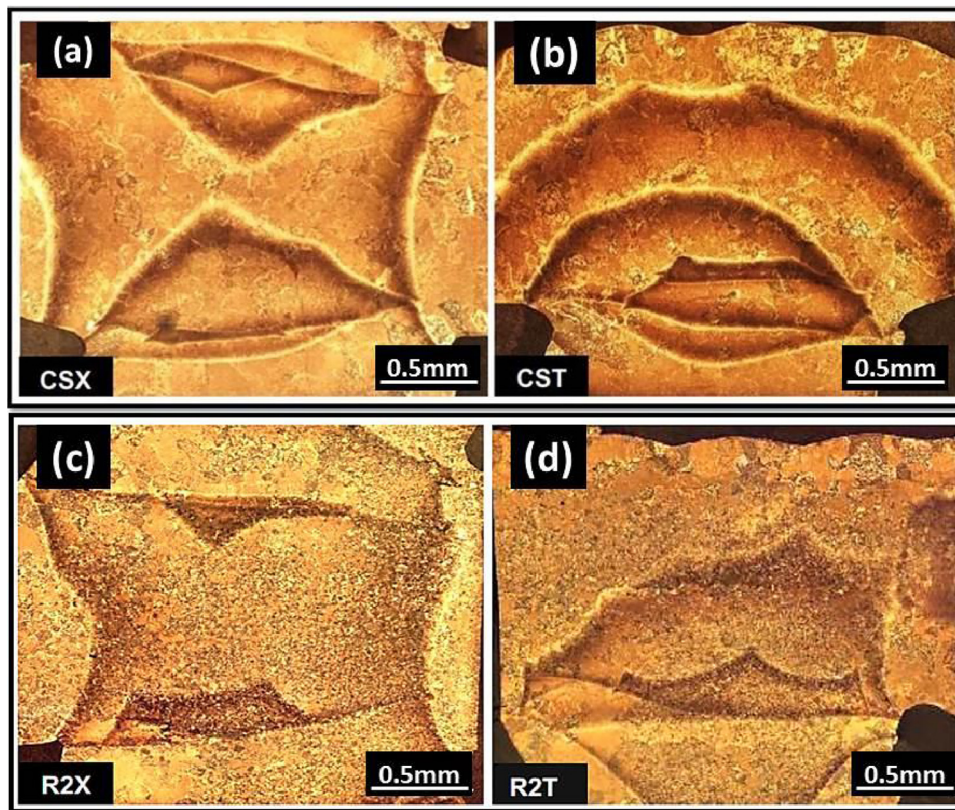**Fig. 10.** (a) Cruciform and (b) tee intersections.

Fig. 11. Metallographic sections from the different intersections showing: (a) unrolled cruciform, (b) unrolled tee, (c) twice rolled cruciform at 75 kN, and (d) twice rolled tee section at 75 kN.
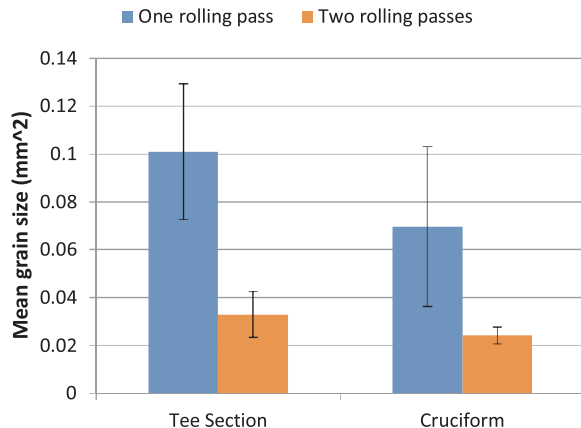

Fig. 12. Mean prior β grain size for the tee and cruciform intersections according to the Planimetric Method (ASTM E-112). Error bars represent ± standard error of the mean.

the unresolved regions of the six β-reconstructed IPF maps were merged into map regions with relatively low to relatively large deviation, representing the plastic strain density. This strain mapping technique based on EBSD β–reconstruction is also explained in more detail in Donoghue et al. [23], who applied this technique successfully to rolled Ti-6Al-4V WAAM walls.

3. Results and discussion

3.1. Thick wall microstructural observations

In Fig. 8, the microstructures of the unrolled sample and a rolled sample are compared. The results clearly show that significant

recrystallisation and refinement of the prior β grains occur when the inverted profile rollers are used to deform the samples. The prior β grain size results are plotted in Fig. 9. The reason why rolling is believed to refine the columnar β-grains, as originally reported elsewhere [6], is due the rolling process generating new β orientations that are able to out-compete growth from the residual β upon reheating above the β transus, thus breaking the columnar grains.

Interestingly, the results in Fig. 9 show that the mean recrystallised grains are larger when a roller with a smaller contact area is used. This phenomenon can be explained by the pressure generated by the rollers. For the smaller radii the pressure was more localised causing a thinner band of recrystallized material. Consequently when the Planimetric Method was used to calculate the mean grain size many larger grains outside of the directly recrystallised area were included in the calculation, which increased the mean grain size calculation. Regardless of the roller type used it can be clearly seen that more recrystallization occurs with larger applied forces.

3.2. Intersection microstructural observations

Photographic images of the cruciform and tee intersections are shown in Fig. 10. Very little surface oxidation was observed (as indicated by surface discolouration) as a consequence of slow deposition and use of the local shielding device which minimised surface oxidation. As an aside, the oxygen content of the thick wall described in Section 3.1 which was also built with the local shielding device indicated that it was between 0.17 (inside) and 0.18 (outside) which was within the 0.12-0.18% limit in the specification for the supplied wire (Table 1). Well-formed intersecting WAAM features that have a uniform layer height are difficult to obtain and require careful control of the deposition parameters around the intersection in particular.

Some of the photos from the metallographic analysis are presented in Fig. 11. As-deposited WAAM titanium is characterised by coarse
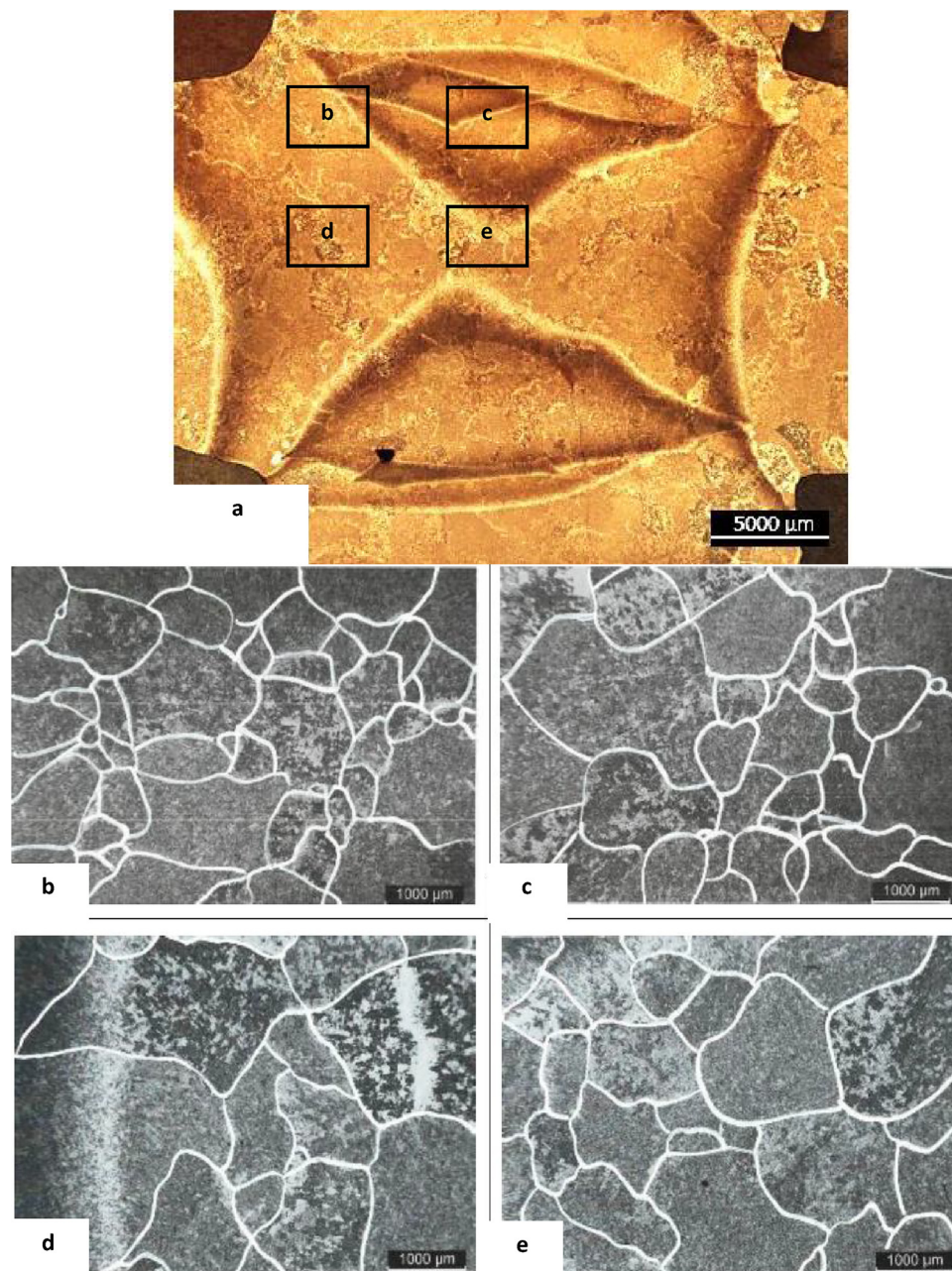
Fig. 13. Microstructure of the cruciform intersection without rolling.

columnar prior β grains that grows epitaxially across the layers; cut samples show the microstructure across the growth direction of the columnar grains (see Fig. 11(a) and (b)). The strain induced by rolling and the heat treatment due to the deposition of the next layer, causes refinement of the grains, as shown in Fig. 11(c) and (d).

The average prior β grain size for the rolled samples is shown in Fig. 12. Please note that due to the columnar grains in the control samples being comparatively large, their mean grain sizes are not displayed (1.28 mm^2 and 1.16 mm^2 for the tee and cruciform, respectively). Comparing the results shows that the second roller pass achieves an average grain size reduction of 67.3% for the tee intersection and 65.7% for the cruciform intersection compared to the single pass rolling strategy. In addition, the average grain size values are slightly smaller in the cruciform intersection compared to the tee intersection. The cooling rates with this geometry are likely to be slightly greater due to the greater heat sink caused by the larger amount of material around the intersecting feature. The greater cooling rate

produces a more refined microstructure [25]. Fig. 12 also shows that the variation of the grain size was reduced with two roller passes, as evidenced by the smaller error bars.

Higher magnification images of the unrolled and rolled cruciform intersections are shown in Fig. 13 and Fig. 14, respectively. The grain size is not uniform across the intersections that were rolled, although, as previously stated there was less variation when two roller passes were applied. The smallest grains are found where the rolling paths cross (Fig. 14(c) and (e)); while the largest grains are outside the rolled region (Fig. 14(b)); and there is a slight grain size increase between the roller paths Fig. 14(d). Similar results were obtained for the tee Intersection.

3.3. EBSD and strain mapping

The EBSD maps are shown in Fig. 15. The IPF of the α-phase (Fig. 15(a)) shows that most of the anisotropic hcp crystals are
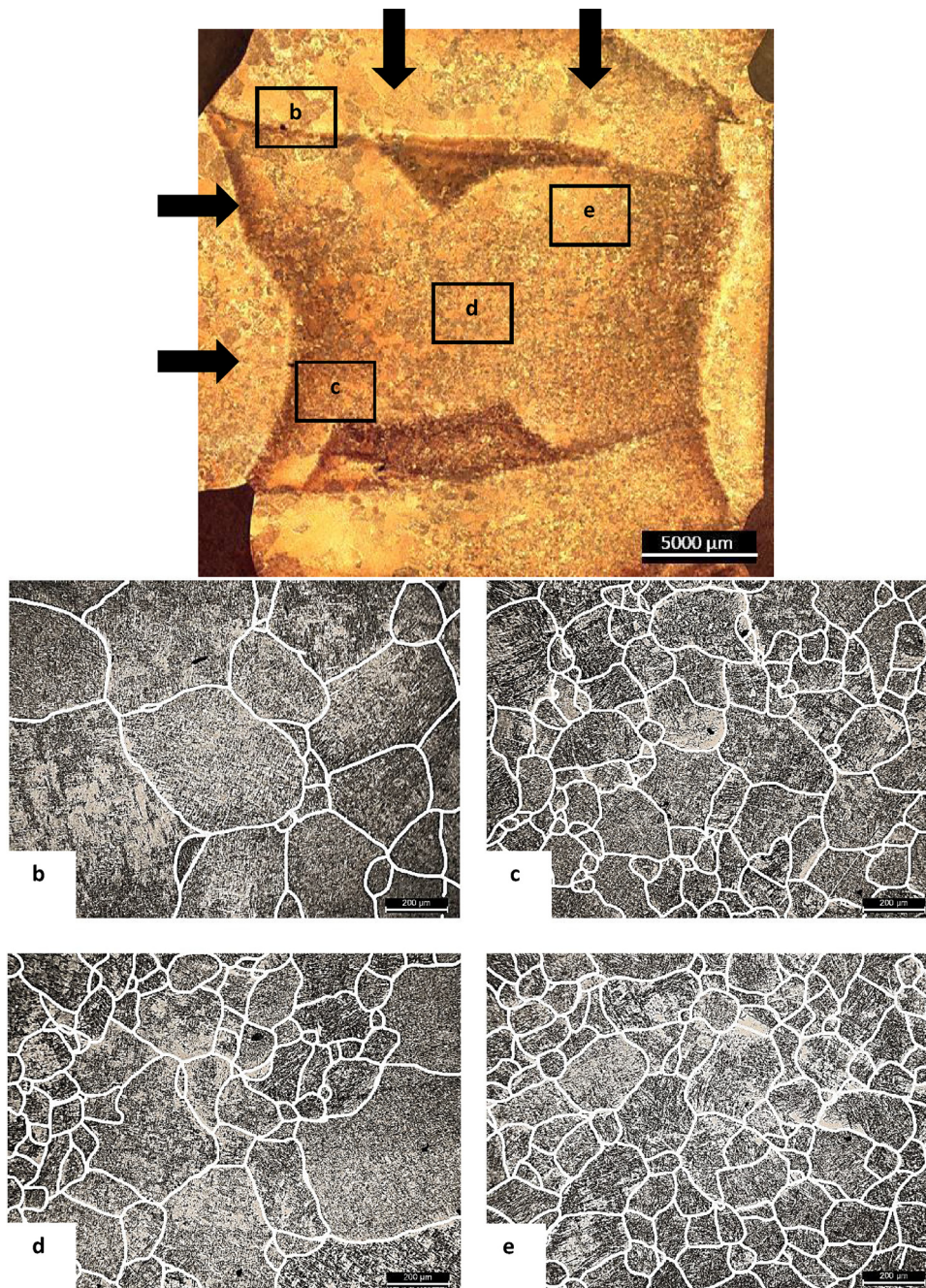
Fig. 14. Microstructure of the cruciform intersection rolled with two roller passes. Note that the arrows show the location of the roller passes.

predominantly oriented with the {110} or the {102} plane normal to the build direction z. These two dominant alignments are typical for Ti-6Al-4V WAAM [23]. Fig. 15(b) is an example of the reconstructed β-IPF using 3° deviation tolerance. At the black spots, the reconstruction was not successful, since the deviation was greater than 3°. The plastic strain map is shown in Fig. 15(c). The incremental colouration shows mismatches of neighbouring α-laths as a deviation angle [°] from fulfilling the ideal BOR during β-reconstruction, where a greater angle represents qualitatively a larger plastic deformation. The largest deformation appears at the edges of the rolled groove and reaches a depth of approximately 3 mm. In the centre of the groove at the interface with the roller, a small region of little plastic deformation can be seen, which is where the friction between roller and surface prevented the material from local straining. This effect has been reported elsewhere [26].

This plastic deformation is desired, as it is required to provide the

grain refinement, triggered by the re-heating above β-transus during the deposition of the subsequent layer. Therefore, if the HAZ of one layer overlaps with the region that has been plastically deformed during the previous rolling step, the microstructure will be refined. It should be noted that the EBSD maps don't show the actual plastic strain, but indicate qualitatively the local strain density.

No noteworthy plastic deformation occurs outside the edges of the groove in the transverse y-direction. i.e. the width of the rolled grove is the same as the width of the plastic deformation within the material. Therefore, for the path planning of multiple rolling passes the following conclusion can be drawn: for a comprehensive strain induction and homogeneous grain refinement, the step distance of parallel rolling passes should be equal to the width of the groove, produced by a single rolling pass.

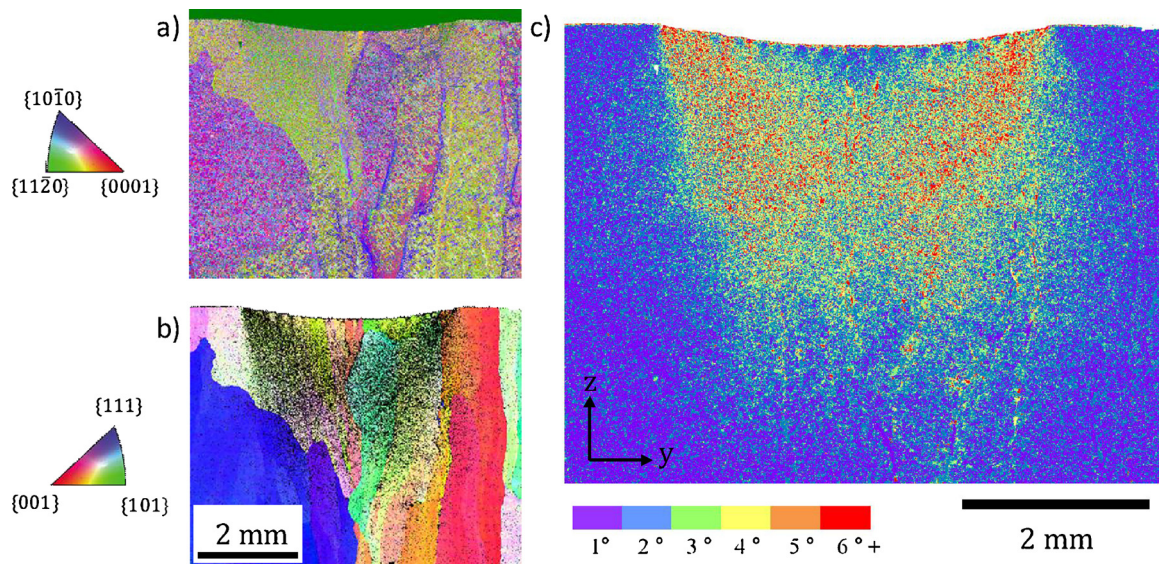The deformation produced by the roller needs to be sufficiently

Fig. 15. EBSD maps of the cross-section under the rolled groove showing the a) IPF colouring of the α-phase orientation in respect to the global z-axis; b) the reconstructed β-orientation; and c) plastic strain map (the deviation of neighbouring α-crystals from fulfilling the ideal BOR).

large to extend into the heat affected zone of the next deposited layer. i.e. deformation at the surface is of little value because it will be melted with the next deposited layer. Fig. 10(b) shows that the banding in the heat affected zone extends about 6 mm from the top surface in the centre of the specimen. The minimum penetration for the deformation needs to be the remelting depth plus the newly deposited layer height – between 2–2.5 mm, which is achieved with the 3 mm deformation depth indicated in Fig. 15. Subsequent studies will explore the relationship between the location of the deformed material and the heat treatment from the next deposited layer.

4. Conclusions

Results from this research have significant benefits in the development of the wire + arc additive manufacturing (WAAM) technology for the production of aerospace components. This study proves:

- Grain refinement can be achieved via interpass rolling of wide walls and intersecting WAAM features through the application of an inverted profiled roller.
- The different roller types and applied forces have a significant effect on the mean grain size and distribution. The larger rolling forces produced more refinement, while increasing the radius of the roller protrusion increased the extent of the recrystallised area.
- EBSD strain maps showed that the majority of the strain is generated towards the edges of the rolled groove and up to 3 mm below the rolled surface − where it was needed for grain refinement.
- Since the width of the strained region and the groove are almost identical, a uniformly refined microstructure is likely to be produced by setting the step distance equal to the width of the rolled groove.

Acknowledgements

References

[1] Cranfield University, www.waammat.com, (2017).
[2] S.W. Williams, F. Martina, A.C. Addison, J. Ding, G. Pardal, P. Colegrove, Wire + arc additive manufacturing, Mater. Sci. Technol. 32 (2016) 641–647, http://dx.doi.org/10.1179/1743284715Y.0000000073.
[3] D. Ding, Z. Pan, D. Cuiuri, H. Li, Wire-feed additive manufacturing of metal components: technologies, developments and future interests, Int. J. Adv. Manuf. Technol. 81 (2015) 465–481, http://dx.doi.org/10.1007/s00170-015-7077-3.
[4] F. Martina, Investigation of Methods to Manipulate Geometry, Microstructure and Mechanical Properties in Titanium Large Scale wire + arc Additive Manufacturing, Cranfield University, 2014.
[5] P.A. Colegrove, A.R. McAndrew, J. Ding, F. Martina, P. Kurzynski, S. Williams, System architectures for large scale wire + arc Additive Manufacture, 10th Int Conf. Trends Weld. Res. Tokyo, 2016.
[6] P.A. Colegrove, J. Donoghue, F. Martina, J. Gu, P. Prangnell, J. Hönnige, Application of bulk deformation methods for microstructural and material property improvement and residual stress and distortion control in additively manufactured components, Scr. Mater. 135 (2017) 111–118, http://dx.doi.org/10.1016/j.scriptamat.2016.10.031.
[7] F. Martina, P.A. Colegrove, S.W. Williams, J. Meyer, Microstructure of interpass rolled wire + arc additive manufacturing Ti-6Al-4V components, Metall. Mater. Trans. A 46 (2015) 6103–6118, http://dx.doi.org/10.1007/s11661-015-3172-1.
[8] J. Gu, J. Ding, S.W. Williams, H. Gu, P. Ma, Y. Zhai, The effect of inter-layer cold working and post-deposition heat treatment on porosity in additively manufactured aluminum alloys, J. Mater. Process. Technol. 230 (2016) 26–34, http://dx.doi.org/10.1016/j.jmatprotec.2015.11.006.
[9] F. Wang, S. Williams, P. Colegrove, A.A. Antonysamy, Microstructure and mechanical properties of wire and arc additive manufactured Ti-6Al-4V, Metall. Mater. Trans. A Phys. Metall. Mater. Sci. 44 (2013) 968–977 http://www.scopus.com/inward/record.url?eid=2-s2.0-84877582096&partnerID=40&md5=12332c9b71fbc7fd4bd822e1489ae901.
[10] J. Donoghue, A.A. Antonysamy, F. Martina, P.A. Colegrove, S.W. Williams, P.B. Prangnell, The effectiveness of combining rolling deformation with wire-arc additive manufacture on β-grain refinement and texture modification in Ti-6Al-4V, Mater. Charact. 114 (2016) 103–114, http://dx.doi.org/10.1016/j.matchar.2016.02.001.
[11] J.M. Donoghue, Hybrid Additive Manufacture and Deformation Processing for Large Scale Near-Net Shape Manufacture of Titanium Aerospace Components (PhD Thesis), University of Manchester, 2016.
[12] P.A. Colegrove, H.E. Coules, J. Fairman, F. Martina, T. Kashoob, H. Mamash, L.D. Cozzolino, Microstructure and residual stress improvement in wire and arc additively manufactured parts through high-pressure rolling, J. Mater. Process. Technol. 213 (2013) 1782–1791, http://dx.doi.org/10.1016/j.jmatprotec.2013.04.012.
[13] H. Zhang, X. Wang, G. Wang, Y. Zhang, Hybrid direct manufacturing method of metallic parts using deposition and micro continuous rolling, Rapid Prototyp. J. 19 (2013) 387–394, http://dx.doi.org/10.1108/RPJ-01-2012-0006.
[14] X. Zhou, H. Zhang, G. Wang, X. Bai, Y. Fu, J. Zhao, Simulation of microstructure evolution during hybrid deposition and micro-rolling process, J. Mater. Sci. 51 (2016) 6735–6749, http://dx.doi.org/10.1007/s10853-016-9961-0.
[15] Y. Xie, H. Zhang, F. Zhou, Improvement in geometrical accuracy and mechanical property for arc-based additive manufacturing using metamorphic rolling mechanism, J. Manuf. Sci. Eng. 138 (2015), http://dx.doi.org/10.1115/1.4032079.

[16] J.R. Hönnige, S. Williams, M.J. Roy, P. Colegrove, S. Ganguly, Residual stress characterization and control in the additive manufacture of large scale metal structures, 10th Int Conf. Residual Stress, Sydney, 2016.

[17] M.A. Rosales, A. Crochemore, K. Eyitayo, R. Fayolle, I. Stan, P. Sukrongpang, Manufacture of Titanium Aerospace Test Parts with a Local Shielding Device (MSc Group Thesis), Cranfield University, 2016.

[18] G.A. Sargent, K.T. Kinsel, A.L. Pilchak, A.A. Salem, S.L. Semiatin, Variant selection during cooling after beta annealing of Ti-6Al-4V ingot material, Metall. Mater. Trans. A 43A (2012) 3570–3585, http://dx.doi.org/10.1007/s11661-012-1245-y.

[19] P. Davies, W. Kockelmann, B. Wynne, R. Eccleston, B. Hutchinson, W.M. Rainforth, Validation of neutron texture data on GEM at ISIS using electron backscattered diffraction, Meas. Sci. Technol. 19 (2008) 34002, http://dx.doi.org/10.1088/0957-0233/19/3/034002.

[20] P.S. Davies, B.P. Wynne, W.M. Rainforth, M.J. Thomas, P.L. Threadgill, Development of microstructure and crystallographic texture during stationary shoulder friction stir welding of Ti-6Al-4V, Metall. Mater. Trans. A 42A (2011) 2278–2289, http://dx.doi.org/10.1007/s11661-011-0606-2.

[21] M. Humbert, N. Gey, The calculation of a parent grain orientation from inherited variants for approximate (b.c.c. − h.c.p.) orientation relations research papers, J. Appl. Crystallogr. (2002) 401–405, http://dx.doi.org/10.1107/S0021889802005824.

[22] T.E. Buchheit, G.W. Wellman, C.C. Battaile, Investigating the limits of polycrystal plasticity modeling, Int. J. Plast. 21 (2005) 221–249, http://dx.doi.org/10.1016/j.ijplas.2003.10.009.

[23] J. Donoghue, A.A. Antonysamy, F. Martina, P.A. Colegrove, S.W. Williams, P.B. Prangnell, The effectiveness of combining rolling deformation with wire-arc additive manufacture on β-grain refinement and texture modification in Ti-6Al-4V, Mater. Charact. (2016), http://dx.doi.org/10.1016/j.matchar.2016.02.001.

[25] P. Åkerfeldt, M.-L. Antti, R. Pederson, Influence of microstructure on mechanical properties of laser metal wire-deposited Ti-6Al-4V, Mater. Sci. Eng. A. 674 (2016) 428–437, http://dx.doi.org/10.1016/j.msea.2016.07.038.

[26] L.D. Cozzolino, H.E. Coules, P.A. Colegrove, S. Wen, Investigation of post-weld rolling methods to reduce residual stress and distortion, J. Mater. Process. Technol. 247 (2017) 243–256.